Journal of Biomedical Optics

SPIEDigitalLibrary.org/jbo

Measurement of oxygen saturation in small retinal vessels with adaptive optics confocal scanning laser ophthalmoscope

Hao Li
Jing Lu
Guohua Shi
Yudong Zhang

SPIE

Measurement of oxygen saturation in small retinal vessels with adaptive optics confocal scanning laser ophthalmoscope

Hao Li, Jing Lu, Guohua Shi, and Yudong Zhang
The Key Laboratory on Adaptive Optics, Graduate School of Chinese Academy of Sciences, Institute of Optics and Electronics, Chengdu 610209, China

Abstract. We have used an adaptive optics confocal scanning laser ophthalmoscope to assess oxygen saturation in small retinal vessels. Images of the vessels with a diameter smaller than 50 μm are recorded at oxygen sensitive and isosbestic wavelengths (680 and 796 nm, respectively). The vessel optical densities (ODs) are determined by a computer algorithm. Then, OD ratios (ODRs), which are inversely proportional to oxygen saturation, are calculated. The results show that arterial ODRs are significantly smaller than venous ODRs, indicating that oxygen saturation in the artery is higher than that in the vein. To the best of our knowledge, this is the first noninvasive measurement of oxygen saturation in small retinal vessels. [DOI: 10.1117/1.3655354]

Keywords: adaptive optics confocal scanning laser ophthalmoscope; retinal oximetry; retinal image registration; spectrophotometry.

Paper 11443LR received Aug. 16, 2011; revised manuscript received Sep. 20, 2011; accepted for publication Oct. 3, 2011; published online Nov. 10, 2011.

The retina has a high demand for oxygen, and retinal hypoxia is believed to be an important factor in retinal diseases, such as diabetic retinopathy,[1] glaucoma,[2] and arteriovenous occlusion.[3] Because retinal microvasculature plays an important role in the oxygen supply, the measurement of the oxygen saturation in small retinal vessels would be very useful to diagnose and monitor these diseases.

A lot of noninvasive techniques have been developed to measure the oxygen saturation of retina. Hickham et al. were the first to noninvasively measure the retinal oxygenation using photographic methods.[4] Delori developed a three-wavelength oximetry to obtain oxygen saturation in retinal vessels.[5] Beach et al. presented a digital imaging system to measure oxygen saturation in retinal vessels by dual-wavelength imaging.[6] Khoobehi et al. developed a hyperspectral imaging technique for spatially mapping the relative oxygen saturation in the optic nerve head.[7] Narasimha-Iyer et al. developed automatic algorithms for oximetry with dual-wavelength fundus images.[8] Ramella-Roman et al. introduced a multiaperture camera system for oxygen saturation measurement in retinal vessels.[9] Kagemann et al. used Fourier domain optical coherence tomography to assess retinal oxygen saturation, and a difference between arterial and venous oxygen saturation was detected.[10] Smith et al. used a scanning laser ophthalmoscope to measure retinal oxygen saturation in vessels with a diameter larger than 50 μm.[11]

However, the image resolution of the above mentioned methods is restricted by ocular aberrations. For the vessels smaller than 50 μm, the image difference between different wavelengths and the vessel profile are difficult to be detected. Thus, it is very difficult to measure oxygen saturation in the vessels smaller than 50 μm,[5,6,11] though the small vessels can be imaged. On the other hand, the ocular aberrations can be compensated with adaptive optics (AO) to achieve a nearly diffraction-limited resolution.[12] AO has been combined with confocal scanning laser ophthalmoscope (AOSLO)[13–15] to improve the imaging resolution.

In this study, oxygen saturation in small retinal vessels with diameters ranging from 27 to 49 μm is assessed by AOSLO. High resolution retinal vessel images are obtained at oxygen sensitive and isosbestic wavelength (680 and 796 nm, respectively). Optical densities (ODs) of vascular segments are determined by a computer algorithm. Then, the OD ratios (ODRs) that are inversely proportional to the oxygen saturation are calculated.

A dual-wavelength AOSLO system for real-time (30 Hz) retina imaging is used in the experiment. Figure 1 shows a schematic diagram of the setup. A band-filtered beam (680 or 796 nm, 7 nm bandwidth) of light emitted from a superluminescent diode (SLD1: Superlumdiodes Ltd., SLD-261-HP or SLD2: Superlumdiodes Ltd., SLD-381-HP1) is focused to a small spot on the retina. Two scanning mirrors [horizontal scanner (HS): 16 KHz resonant scanner, Electro-Optical Products Corp. vertical scanner (VS): 30 Hz galvometric scanner, Cambridge 6800-HP-3YS] are used to control the focused spot to scan the retina. Light scattered back from the retina is split into two beams. One beam enters a photomultiplier tube (PMT, Hamamatsu H7422-20) for signal detection. By synchronizing the PMT signal and two scanning mirrors, the retinal images can be consecutively recorded. The other beam is captured by a Shack–Hartmann wavefront sensor (WS) with 97 effective subapertures in 11×11 arrays. The slope data of the wavefront are acquired by a computer and transferred to control signals for a 37-channel deformable mirror (DM). After 20 to 30 iterations, the error of the corrected wavefront approaches the minimum. The resolution of our imaging system is approximately 2.5 μm lateral and better than 100 μm axial.[15]

Eight normal healthy volunteers (3 female, 5 male, ages range from 22 to 30 years) were recruited for this study. To control the image location, a computer-controlled 8×8 LED array fixation target was provided for the volunteer to view while imaging. In order to find the best imaging plane of blood vessels, defocus was applied to section the retina axially. Video clips of retinal vessels at 680 and 796 nm were recorded sequentially. The frame size is 512×480 pixels, and the field of view is 1.5 deg. The time interval between two wavelengths switching is approximately 3 s. Four sequential frames were averaged to improve the image quality.[16]

Address all correspondence to: Guohua Shi, Institute of Optics and Electronics, Chinese Academy of Sciences, Shuangliu P.O. Box 350, Chengdu 610209, China; Tel: +8613880184201; Fax: +86028-85100433; E-mail: guohua_shi@yahoo.com.cn.

1083-3668/2011/16(11)/110504/3/$25.00 © 2011 SPIE

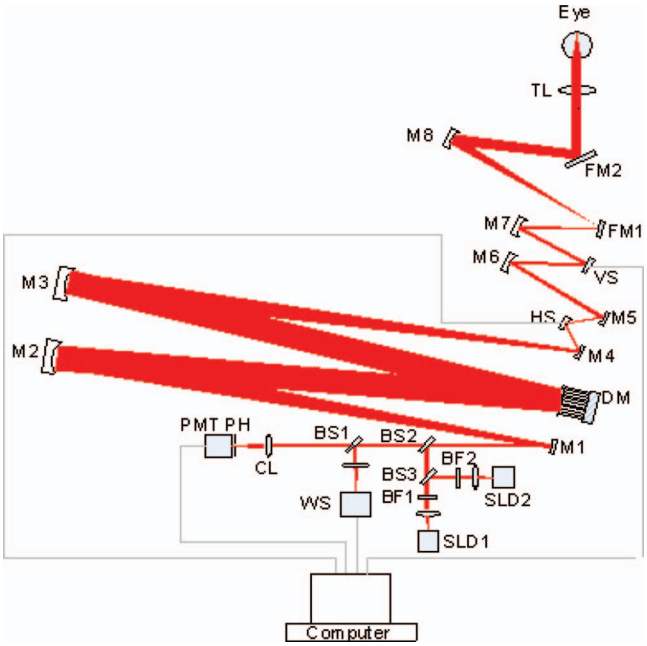

Fig. 1 Schematic of a dual-wavelength AOSLO system. HS, horizontal scanner; VS, vertical scanner; WS, wavefront sensor; DM, deformable mirror; PMT, photomultiplier tube; BS1, BS2, BS3, beam splitters; BF1, BF2, band filters; CL, collecting lens; FM1, FM2, folding mirrors; SLD1, SLD2, superluminescent diodes; M1 ~ M8, spherical mirrors; PH, pinhole; TL, trial lens.

Due to the eye motion, the retinal images at different wavelengths have to be registered. The similarity between the images at 680 and 796 nm is determined using mutual information,[17] which is defined as

$$I(A, B) = \sum_{i,j} p_{AB}(i, j) \log \frac{p_{AB}(i, j)}{p_A(i, j) \cdot p_B(i, j)}, \quad (1)$$

where $p_{AB}(i, j)$ is the joint probability distribution of images A and B, and $p_A(i, j)$ and $p_B(i, j)$ are probability distributions of images A and B, respectively. $p_{AB}(i, j)$ can be estimated by calculating a normalized joint histogram of the gray values, and $p_A(i, j)$ and $p_B(i, j)$ can be estimated by calculating a normalized histogram.[17] The image at 680 nm was used as a reference. A subimage from the image at 796 nm was translated and rotated to maximize $I(A,B)$ of the subimage and the reference image. Then, the translation and the rotation of the image at 796 nm were determined, and the images were registered.

After the registration, a computer program was used to obtain the paths by tracking the minimum intensity inside the vessel and the outside intensity at a fixed distance from the minimum intensity. The paths were identified in the 796 nm images, and the corresponding paths on the 680 nm images were also determined. The results are shown in Fig. 2. Figures 2(a) and 2(c) were acquired at 680 nm, and Figs. 2(b) and 2(d) were acquired at 796 nm. The diameters of the vessels in Figs. 2(a) and 2(c) are approximately 49 and 34 μm, respectively. The vessel diameter was determined by the method described in Ref. 5. Then, a direct calculation of the vessel OD was obtained at wavelength λ by averaging the intensities on the paths inside and outside the vessels ($I_{\lambda \text{in}}$ and $I_{\lambda \text{out}}$).

$$\text{OD}_\lambda = \log_{10}(I_{\lambda \text{out}} / I_{\lambda \text{in}}). \quad (2)$$

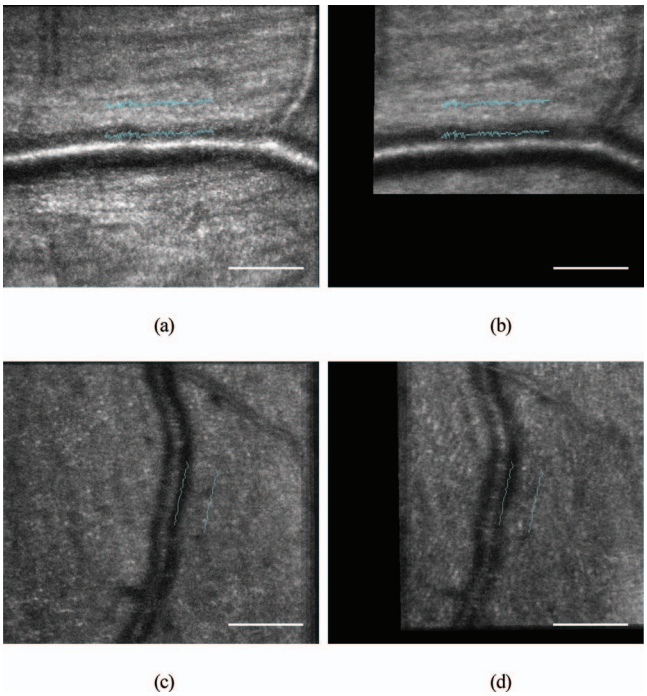

Fig. 2 The paths tracked along the retinal vessels. (a) and (c) Retinal images acquired at 680 nm. (b) and (d) Retinal images acquired at 796 nm. All scale bars represent 100 μm.

The ODRs between the ODs measured at oxygen sensitive wavelength and isosbestic wavelength bear an inverse linear relationship to oxygen saturation.[4,6,8,11] ODR is expressed as:

$$\text{ODR} = \text{OD}_{\text{sensitive}} / \text{OD}_{\text{isosbestic}}. \quad (3)$$

The extinction coefficients of HbO_2 and Hb vary with wavelength.[18] At 680 nm, the difference in extinction coefficients between HbO_2 and Hb is relatively large, while at 796 nm the difference is small. For this reason, 680 nm was used as the oxygen sensitive wavelength, and 796 nm was used as the isosbestic wavelength. $\text{OD}_{680\text{ nm}}/\text{OD}_{796\text{ nm}}$ follows an inverse linear relationship with oxygen saturation. The calculated ODRs of the vessels in Fig. 2 are presented in Table 1.

As is shown in Table 1, vascular ODR in Fig. 2(a) is significantly smaller than that in Fig. 2(c). This suggests that the vascular oxygen saturation in Fig. 2(a) is higher than that in Fig. 2(a).

A fundus camera (Cannon CR6-45NM) was used to identify retinal arteries and veins. A fundus camera image is shown in Fig. 3, and the field of view is 37 deg. The black and white rectangles in Fig. 3 represent the regions in Figs. 2(a) and 2(c), respectively. Arteries and veins were identified by visual inspection of the fundus camera image. The vessel in Fig. 2(a) is an

Table 1 ODRs of the vessels in Fig. 2.

Figures	OD_{680}	OD_{796}	ODR
2(a)	0.27	0.49	0.55
2(c)	0.46	0.48	0.96

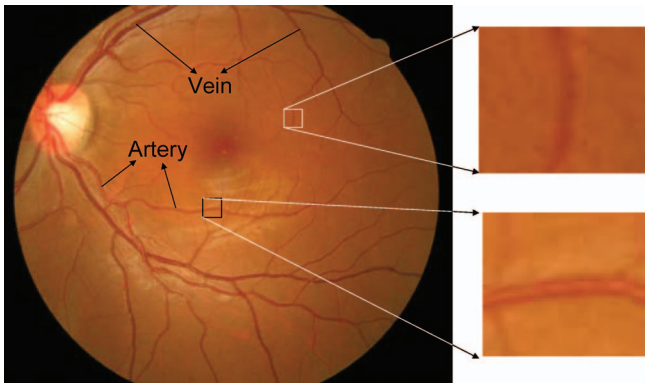

Fig. 3 A fundus camera image showing the same regions imaged in Fig. 2.

artery and the vessel in Fig. 2(c) is a vein. Thus, the vascular oxygen saturation in Fig. 2(a) is higher than that in Fig. 2(c). This agrees with the results obtained with AOSLO.

ODRs of the eight volunteers' vessels are presented in Table 2, and the results show that the arterial ODRs are significantly smaller than the venous ODRs (0.60 ± 0.11 and 0.98 ± 0.07, respectively; $p < 0.00001$) (mean $\pm$ standard deviation). A significant difference between arterial and venous oxygen saturation is therefore detected.

In summary, AOSLO has been used to assess retinal oxygen saturation. The retinal vessels with diameter ranging from 27 to 49 μm were imaged at two wavelengths (680 and 796 nm), and the ODRs of the vessels between 796 and 680 nm were calculated. The results showed that arterial ODRs were significantly smaller than venous ODRs, indicating that oxygen saturation in the artery is higher than that in the vein. As the oxygen saturation in small vessels can be affected by the metabolic activity in the local areas of the retina, the measurement of the oxygen saturation would be very useful to achieve early assessments of retinal disease associated with oxygen utilization.

Table 2 Comparison of arterial and venous ODRs.

	Artery		Vein	
	Diameter (μm)	ODR	Diameter (μm)	ODR
1	49	0.55	34	0.96
2	46	0.69	33	0.95
3	47	0.43	29	0.93
4	32	0.51	37	1.09
5	38	0.60	43	1.06
6	27	0.77	38	0.93
7	31	0.58	47	0.88
8	49	0.68	31	1.00

Acknowledgments

This research was supported by the Knowledge Innovation Program of the Chinese Academy of Sciences, Grant No. KGCX2-Y11-920.

References

1. E. Stefansson, M. B. Landers, and M. L. Wolbarsht, "Oxygenation and vasodilatation in relation to diabetic and other proliferative retinopathies," *Ophthalmic Surg.* **14**(3), 209–226 (1983).
2. S. Blumenröder, A. J. Augustin, and F. H Koch, "The influence of intraocular pressure and systemic oxygen tension on the intravascular pO2 of the pig retina as measured with phosphorescence imaging," *Surv. Ophthalmol.* **42**(Supp l), S118–S126 (1997).
3. S. Yoneya, T. Saito, Y. Nishiyama, T. Deguchi, M. Takasu, T. Gil, and E. Horn, "Retinal oxygen saturation evels in patients with central retinal vein occlusion," *Ophthalmology* **109**(8), 1521–1526 (2002).
4. J. B. Hickam, R. Frayser, and J. C. Ross, "A study of retinal venous blood oxygen saturation in human subjects by photographic means," *Circulation* **27**, 375–385 (1963).
5. F. C. Delori, "Noninvasive technique for oximetry of blood in retinal vessels," *Appl. Opt.* **27**(6), 1113–1125 (1988).
6. J. M. Beach, K. J. Schwenzer, S. Srinivas, D. Kim, and J. S. Tiedeman, "Oximetry of retinal vessels by dual-wavelength imaging: calibration and influence of pigmentation," *J. Appl. Physiol.* **86**(2), 748–758 (1999).
7. B. Khoobehi, J. M. Beach, and H. Kawano, "Hyperspectral imaging for measurement of oxygen saturation in the optic nerve head," *Invest. Ophthalmol. Visual Sci.* **45**(5), 1464–1472 (2004).
8. H. Narasimha-lyer, J. M. Beach, B. Khoobehi, J. Ning, H. Kawano, and B. Roysam, "Algorithms for automated oximetry along the retinal vascular tree from dual-wavelength fundus images," *J. Biomed. Opt.* **10**(5), 054013 (2005).
9. J. C. Ramella-Roman, S. A. Mathews, H. Kandimalla, A. Nabili, D. D. Duncan, S. A. D'Anna, S. M. Shah, and Q. D. Nguyen, "Measurement of oxygen saturation in the retina with a spectroscopic sensitive multi aperture camera," *Opt. Express* **16**(9), 6170–6182 (2008).
10. L. Kagemann, G. Wollstein, M. Wojtkowski, H. Ishikawa, K. A. Townsend, M. L. Gabriele, V. J. Srinivasan, J. G. Fujimoto, and J. S. Schuman, "Spectral oximetry assessed with high-speed ultra-high-resolution optical coherence tomography," *J. Biomed. Opt.* **12**(4), 041212 (2007).
11. M. H. Smith, K. R. Denninghoff, L. W. Hillman, and R. A. Chipman, "Oxygen saturation measurements of blood in retinal vessels during blood loss," *J. Biomed. Opt.* **3**(3), 296–303 (1998).
12. A. Roorda and D. R. Williams, "The arrangement of the three cone classes in the living human eye,"*Nature* **397**(679), 520–522 (1999).
13. A. Roorda, F. Romero–Borja, W. J. Donnelly, H. Queener, T. J. Hebert, and M. C. W. Campbell, "Adaptive optics scanning laser ophthalmoscopy," *Opt. Express* **10**(9), 405–412 (2002).
14. D. X. Hammer, R. D. Ferguson, C. E. Bigelow, N. V. Iftimia, T. E. Ustun, and S. A. Burns, "Adaptive optics scanning laser ophthalmoscope for stabilized retinal imaging," *Opt. Express* **14**(8), 3354–3367 (2006).
15. J. Lu, H. Li, L. Wei, G. Shi, and Y. Zhang. "Retina imaging in vivo with the adaptive optics confocal scanning laser ophthalmoscope," *Proc. SPIE* **7519**, 75191I (2009).
16. H. Li, J. Lu, G. Shi, and Y. Zhang, "Tracking features in retinal images of adaptive optics confocal scanning laser ophthalmoscope using KLT-SIFT algorithm," *Biomed. Opt. Express* **1**(1), 31–40 (2010).
17. C. Studholme, D. L. G. Hill, and D. J. Hawkes, "An overlap invariant entropy measure of 3D medical image alignment," *Pattern Recogn.* **32**(1), 71–86 (1999).
18. Data tabulated from various sources compiled by S. Prahl, http://omlc.ogi.edu/spectra.